Flooded-area satellite monitoring within a Ramsar wetland Nature Reserve in Argentina

Anabella Ferral[a,b], Eduardo Luccini[c,d,*], Alejandro Aleksinkó[e], Carlos M. Scavuzzo[a]

[a] Instituto Gulich, Universidad Nacional de Córdoba-CONAE, Centro Espacial Teófilo Tabanera, Ruta 45 km 8, Falda del Cañete, 5187, Córdoba, Argentina
[b] Cátedra UNESCO en Seguridad Humana y Desarrollo Regional & CIADE-CdA, Universidad Blas Pascal, Av. Donato Alvarez 380, 5000, Córdoba, Argentina
[c] CONICET, Centro de Excelencia en Productos y Procesos de Córdoba (CEPROCOR), Sede Santa María de Punilla, Pabellón Ceprocor, X5164, Córdoba, Argentina
[d] Pontificia Universidad Católica Argentina, Facultad de Química e Ingeniería del Rosario, Av. Pellegrini 3314, 2000, Rosario, Argentina
[e] Secretaría de Recursos Hídricos y Coordinación de la Provincia de Córdoba, Humberto Primo 607, 5000, Córdoba, Argentina

A R T I C L E   I N F O

A B S T R A C T

The protection and restoration of water-related ecosystems is one of the goals to be achieved by the United Nations' 2030 Agenda for Sustainable Development. In this framework and requested by government Argentine institutions concerned with water, biodiversity and territorial management, this study analyzes the evolution of the flooded area within the *Dulce River wetlands and Mar Chiquita Lake* Nature Reserve (centered around 30.6°S, 62.6°W, 70 m above sea level) in Argentina since 2003, when the historical maximum extent was reached, until 2017. The Modified Normalized Difference Water Index (MNDWI) was calculated on atmospherically corrected NASA Landsat 5 Thematic Mapper (L5-TM) and Landsat 8 Operational Land Imager (L8-OLI) reflectance data over two-scene cloudless-sky mosaics to cover the whole Reserve. Mixed-water pixels constituted an important fraction of the total-water covered area, particularly during years of minimum water level in Mar Chiquita Lake. So, MNDWI values were analyzed along transects crossing two stable regional water bodies to determine precise thresholds for detection of non-water (MNDWI < -0.15 for L5-TM, MNDWI < -0.35 for L8-OLI), mixed-water ($-0.15 <$ MNDWI < 0.4 for L5-TM, $-0.35 <$ MNDWI < 0.5 for L8-OLI) and open-water ($0.4 <$ MNDWI for L5-TM, $0.5 <$ MNDWI for L8-OLI) pixels. A higher spatial resolution image, SPOT5-HGR2, was used to validate the classification method. A confusion matrix was built which resulted in an overall accuracy of 99.2% and a Kappa coefficient of 0.98. In-situ Geo-referenced photographic registers were also taken simultaneously to a Landsat 8 overpass to confirm the classification thresholds. The analysis of simulated MNDWI response, by using the assumption of the linear mixture model, showed that mixed pixels should present from 9% to 76% of detectable open-water area. Maximum total flooded area extensions of about 3600 km² by 2003–2005 and a minimum one of 2050 km² by the end of 2011 were established, followed by a recent trend to the recovering with a total flooded area of about 3400 km² in the period 2015–2017. Open-water covered area follows closely the behavior of in-situ water level measurements of Mar Chiquita Lake, showing a maximum in year 2003 and a minimum towards the end of 2013, in a significant linear relation from which a topographical slope of the terrain of about 0.012% is inferred that agrees with previous bathymetric studies. Results show the powerful complement between a reliable water satellite monitoring tool and locally-measured parameters in so dynamic wetland regions.

1. Introduction

The changes in the extent of water over time on wetlands are an important indicator to be followed, as proposed by the Statistical Commission of the United Nations' 2030 Agenda for Sustainable Development, and remote sensing techniques appear as the best choice to be implemented (UN, 2017). Satellite sensors measurements become a crucial tool in the last decades for tracking different aspects of our planet. Measurements from a variety of wavelength channels, many of which are common to different satellite instruments, have been combined to define a series of specific indices characterizing parameters of interest. Referred to water bodies and particularly to the monitoring of

wetlands, they were applied to a variety of subjects such as environmental assessment (e.g., Mozumder et al., 2014), water volume (Crétaux et al., 2016), hydrological dynamics and flooding (Chen et al., 2013; Sharma et al., 2014; Li et al., 2015; Wang et al., 2015). Since 1972, the National Aeronautics and Space Administration (NASA) Landsat satellite series have produced the longest continuous global record of the Earth's surface. Landsat 8, launched in February 2013, meant a success to assure continuity with Landsat 5 data which was decommissioned in June 2013. In this work, reflectance measurements from both Landsat 5 Thematic Mapper (L5-TM) and Landsat 8 Operational Land Imager (L8-OLI) sensors are used. The Modified Normalized Difference Water Index (MNDWI) (Xu, 2006) is extensively employed from Landsat multispectral radiometers data for the identification of water bodies (e.g., Ji et al., 2009; Xu-kai et al., 2012; Chen et al., 2013; Sharma et al., 2014; Li et al., 2015; Wang et al., 2015). Particularly, Ferral et al. (2013) made one of the first adaptations of the MNDWI to the specific radiometric bands of L8-OLI. The identification of open water bodies from satellite imagery is at present a relatively simple task. However, the accurate delineation of lake shorelines or the determination of mixed pixels within wetlands is definitely more challenging, particularly if imagery from only one satellite is used for, and emphasis on this subject is made in the present work.

The *Dulce River wetlands and Mar Chiquita Lake* in Argentina were declared Nature Reserve by Córdoba Province in 1994, and was incorporated in 2002 to the List of Wetlands of International Importance by the Ramsar Convention on Wetlands (http://www.ramsar.org/). Mar Chiquita is the biggest salt lake in Latin America. Studying their isotopic changes, Piovano et al. (2004) found that low water height levels prevailed during the 200 years previous to the 1970's decade. Earlier registers around year 1900 allude to areas of about 1000 km² (Bucher, 2006, and references therein). In contrast, a predominantly positive hydrological balance has given a notable dynamics to the Mar Chiquita Lake water level during the last four decades (Piovano et al., 2002, 2004; Troin et al., 2010), reaching total open-water covered areas over 6000 km². Several studies addressed different aspects on this system, about its geography (Reati et al., 1996), geochemical composition (Martínez, 1995; Piovano et al., 2002), fauna (Bucher, 1992; Nores, 2011), flora (Stutz and Prieto, 2003) and hydrodynamics (Plencovich, 2011). A complete review of the knowledge on the geography, biodiversity and history of this region was made by Bucher (2006).

Concerned by the complex evolution of the *Dulce River wetlands and Mar Chiquita Lake* and attending to its preservation, this research was requested by Argentine government institutions. Main concerns in this region are the Nature Reserve's ecosystem, the management of the real estate market pressure in their edge, and the hydrological balance in response to the pluvial influx from the northern rivers causing frequent flooding events on the principal cities on the south of Mar Chiquita Lake, mainly Miramar city. For this purpose, the flooded area behavior of the Dulce River wetlands within the Nature Reserve was analyzed spanning the period requested by the government authorities (2003–2017), correlating it with simultaneous locally measured water level of Mar Chiquita Lake whose database covers five decades since November 1967 up to the present. So, the analyzed period 2003–2017 includes the historical maximum water level around 2003 and the lowest minimum water level in forty years of 2013.

2. Materials and methods

2.1. Study area

Fig. 1-left presents the geographical location of the *Dulce River wetlands and Mar Chiquita Lake* Provincial Nature Reserve on an official map, centered around 30.6°S, 62.6°W, 70 m above sea level (asl) in Córdoba Province (demarcated at bottom-left corner), Argentina. It is presently in process to be appointed as National Nature Reserve.

Covering 9770.85 km², it will be the largest of a total of 47 National Nature Reserves in Argentina. Including their tributaries, mainly the Dulce River at north, it is part of one of the largest endorheic systems in the world with a total extension of about 37500 km² (Piovano et al., 2002, 2004). Official cartography can be found at http://www.recursoshidricos.gov.ar/webdrh/_docs/Poster_Sistema_Mar_Chiquita.pdf. The northern gray contour of the Nature Reserve in Fig. 1-right (over a 2013 Landsat 8 mosaic in real colour, RGB-432 combination) highlights the area of study of this work and corresponds specifically to the Dulce River wetlands, a potentially flooded region of 7213.62 km².

The southern gray contour in Fig. 1-right is the region actually defined as Mar Chiquita Lake within the Nature Reserve, with a surface of 2557.23 km² whose limit is defined by a salty crustal contour observed at a water level of about 66 m asl typical until year 1976, when the period of big floods started. The rectangular contours in Fig. 1-right demark the sub-areas of Los Porongos lagoon (northern rectangle) and a South branch of Mar Chiquita Lake (MC South Cove, southern rectangle) used to establish the MNDWI thresholds for the satellite pixels classification. The clear arrow on the Northwest border indicates the zone where a field photographic campaign was made as a complement to validate the satellite classification.

2.2. Satellite data

Orbits of both L5 satellite (March 1984 to January 2013) and L8 satellite (active since February 2013) are circular, sun-synchronous, near-polar at an altitude of 705 km asl. They each cross the equator from north to south at 10:00 a.m. ± 15 min local time on each pass to provide maximum illumination with minimum water vapour present (haze and cloud build-up), making an orbit in about 99 min, completing over 14 orbits per day, and covering the same area on the Earth every 16 days, so that about two images a month are available of a given place. Table 1 shows the characteristics of both L5-TM and L8-OLI sensors.

To build the mosaic covering the whole Nature Reserve under study, two scenes from adjacent satellite paths are needed. Both scenes are separated by at least one week in time and they must present a cloudless-sky, limiting the availability of dates to analyze. Selected atmospherically-corrected, geo-referenced and ortho-rectified images used in this work, provided by the United States Geological Survey, are detailed in Table 2. Specific details about these products can be found in the Landsat 4-7 Surface Reflectance product guide (https://landsat.usgs.gov/sites/default/files/documents/ledaps_product_guide.pdf) and Landsat 8 Surface Reflectance Code (LASRC) product guide (https://landsat.usgs.gov/sites/default/files/documents/lasrc_product_guide.pdf). A SPOT 5-HGR2 image from the Argentine National Commission for Space Activities (CONAE) catalogue was used to perform the main validation procedure as it is explained in the next section.

2.3. Satellite data processing

Satellite reflectance data were processed with Environment for Visualizing Images (ENVI) software version 4.2 (HGS, 2016). The Modified Normalized Difference Water Index (MNDWI) is defined as:

$$MNDWI = \frac{r_{green} - r_{SWIR}}{r_{green} + r_{SWIR}} \tag{1}$$

where r_{green} and r_{SWIR} are the reflectance registered from a given direction by the sensor in the green and short-wave infrared ranges respectively (Xu, 2006). The MNDWI takes values in the range [-1, 1] and works reliably for any multispectral sensor with a green band between 0.5 and 0.6 μm (bands B2 for L5-TM and B3 for L8-OLI, see Table 1) and a SWIR band between 1.55 and 1.75 μm (bands B5 for L5-TM and B6 for L8-OLI, see Table 1), enhancing open-water features for which MNDWI values arrange in a positive mode, while suppressing noise from built-up land, vegetation, and soil whose MNDWI values group in a marked
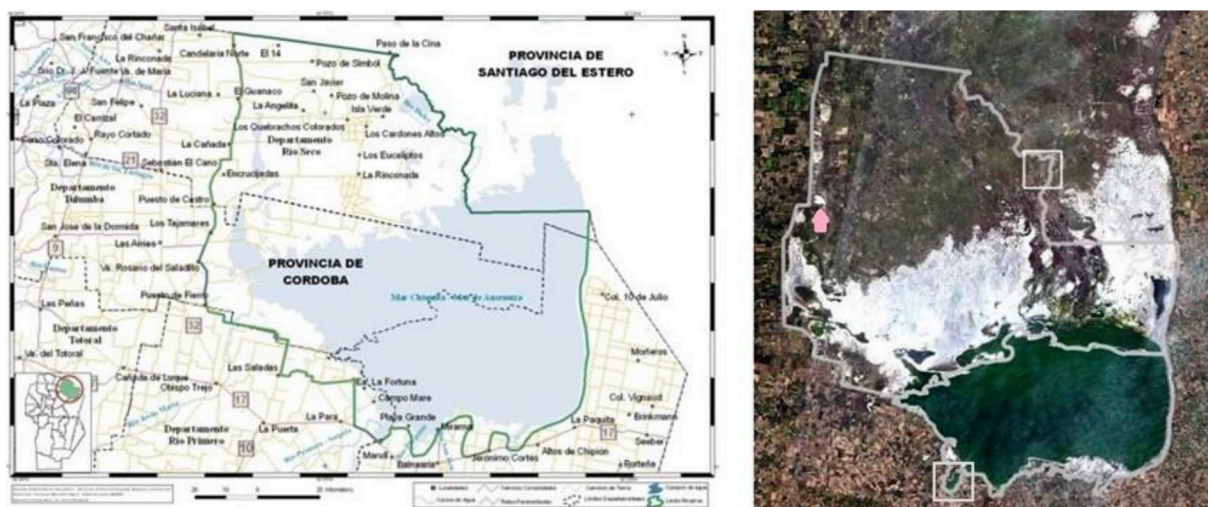
Fig. 1. Left: Geographical location of the *Dulce River wetlands and Mar Chiquita Lake* Nature Reserve (demarked at bottom-left corner) in Córdoba Province, Argentina (source: Argentine Secretary of Environment). Right: The northern gray contour of the Nature Reserve corresponds to the potentially flooded area of Dulce River wetlands analyzed in the present study, highlighted over a 2013 Landsat 8 mosaic in real colour (RGB-432 combination). The southern gray contour is the region actually defined as Mar Chiquita Lake within the Nature Reserve. Rectangular contours correspond to Los Porongos lagoon and a South branch of Mar Chiquita Lake (called MC South Cove), sub-areas used to define the MNDWI thresholds for water pixels classification. The clear arrow on the Northwest border indicates the site where ground photographic registers were taken to validate the satellite pixel classification.

Table 1
Spectral range and spatial resolution of each band (B#) of Landsat 5 Thematic Mapper (L5-TM) and Landsat 8 Operational Land Imager (L8-OLI) sensors. Temporal frequency at a fixed location on the Earth's surface is 16 days.

Sensor	Band	Spectral range [μm]	Spatial resolution [m]
L5-TM	B1	0.45–0.52	30
	B2	0.52–0.60	30
	B3	0.63–0.69	30
	B4	0.76–0.90	30
	B5	1.55–1.75	30
	B6	10.40–12.50	120
	B7	2.08–2.35	30
L8-OLI	B1	0.435–0.451	30
	B2	0.452–0.512	30
	B3	0.533–0.590	30
	B4	0.636–0.673	30
	B5	0.851–0.879	30
	B6	1.566–1.651	30
	B7	2.107–2.294	30
	B8	0.503–0.676	15
	B9	1.363–1.384	30

Table 2
Specifications of the satellite scenes selected in cloudless-sky days along the period 2003–2017 to analyze the extension of the flooded area on the Dulce River wetlands. Each mosaic is constructed from two close-in-date and partially overlapping scenes belonging to satellite paths 228/229 and row 81.

Year of mosaic	Sensor	Scene's date
2003	L5-TM	December 10, 2003
		December 17, 2003
2004	L5-TM	May 02, 2004
		May 09, 2004
2005	L5-TM	March 25, 2005
		April 03, 2005
2006	L5-TM	March 05, 2006
		March 12, 2006
2007	L5-TM	February 04, 2007
		February 11, 2007
2008	L5-TM	October 20, 2008
		October 27, 2008
2009	L5-TM	May 16, 2009
		May 23, 2009
2010	L5-TM	February 03, 2010
		February 12, 2010
2011	L5-TM	March 03, 2011
		March 10, 2011
2011	L5-TM	September 27, 2011
		October 20, 2011
2013	L8-OLI	April 16, 2013
		April 25, 2013
2014	L8-OLI	January 22, 2014
		January 13, 2014
2015	L8-OLI	September 06, 2015
		September 13, 2015
2016	L8-OLI	February 29, 2016
		February 04, 2016
2017	L8-OLI	March 19, 2017
		April 11, 2017
2017	L8-OLI	September 11, 2017
		September 18, 2017

negative mode (e.g., HGS, 2016). The MNDWI thresholds to separate open-water pixels, mixed-water pixels and non-water pixels were obtained through a box-plot analysis of MNDWI values along transects crossing two stable water bodies in the region (Fig. 1-right).

2.4. Classification's precision assessment

A SPOT 5-HRG2 CNES image (spatial resolution 10 m) from 08 April 2018, scene 687/410 was analyzed, using the same thresholds of Table 3 for L8-OLI, to extract check points to be used as ground truth. A confusion matrix was developed to characterise the open-water, mixed-water and non-water pixels classification. Overall accuracy and Kappa coefficient were calculated to assess the accuracy according to equations (e.g. Congalton and Green, 1999):

$$\text{Overall accuracy} = \frac{TP + TN}{T} \tag{2}$$

$$Kappa\ coefficient = \frac{T * (TP + TN) - \Sigma}{T^2 - \Sigma} \tag{3}$$

where *TP* is the number of correctly classified water pixels, *TN* is true negative (the number of correctly rejected non-water pixels), *T* is the total number of evaluated pixels, Σ is the chance accuracy represented by $(TP + FP)(TP + FN) + (FN + TN)(FP + TN)$, *FN* is false negative (the number of undetected water pixels) and *FP* is false positive (the

Table 3
Ranges of MNDWI values established to detect non-water pixels, mixed-water pixels, and open-water pixels in L5-TM and L8-OLI scenes (also shown in Fig. 4).

Surface coverage	L5-TM MNDWI range	L8-OLI MNDWI range
non-water	MNDWI < −0.15	MNDWI < −0.35
mixed-water	−0.15 < MNDWI < 0.4 [a]	−0.35 < MNDWI < 0.5
open-water	0.4 < MNDWI [a]	0.5 < MNDWI

[a] Only in the analysis of L5-TM mosaic of year 2008 the upper threshold was lowered to 0.25 in order to avoid sparse pixels identified as mixed-water within the open-water area of the main lagoon, probably due to strong wind causing waves in the water surface. The threshold of 0.25 was obtained testing the lowest tuned value that assured the correct classification for the totality of open-water pixels within the body of the lagoon.

number of incorrectly extracted water pixels). In addition, photographic registers were taken within the study zone (Fig. 1-right) in simultaneous with a Landsat 8-OLI overpass during April 2015, as a complement to assess the precision of the classification.
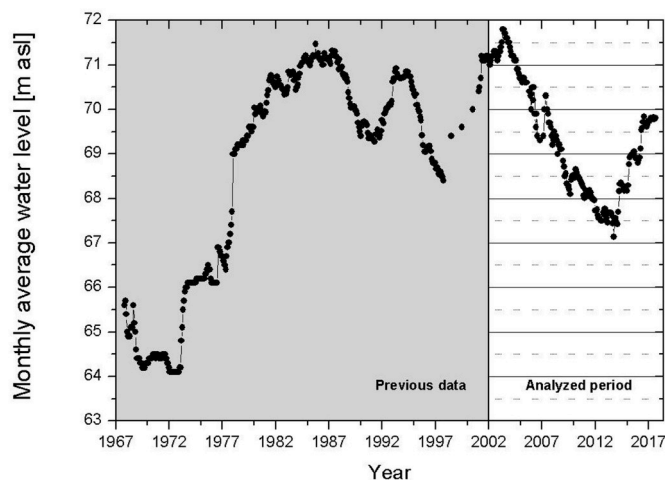
2.5. Water level data

Water height level data of Mar Chiquita Lake are correlated with the satellite-retrieved flooded area. They are daily measured by the *Secretaría de Recursos Hídricos y Coordinación de la Provincia de Córdoba, Argentina*, continuously since November 1967 through a calibrated bar stocked in the lake (e.g. Vargas, 2014).

3. Results and discussion

3.1. Mar Chiquita water level dynamics

Fig. 2 presents the monthly average water height level of Mar Chiquita Lake for the period 1967–2017, noting that it developed a marked dynamical character during the last four decades given the mentioned predominantly positive hydrological balance in its basin (Piovano et al., 2004; Troin et al., 2010).

Since the start of in-situ water level measurements in 1967, the lowest level occurred in 1972 with 64.1 m asl, followed by a systematic increase and an oscillating period afterwards. This work addresses the analysis of the period 2003–2017 which is signed by two roughly linear-in-time steps: the decreasing trend after the historical absolute maximum in May 2003 from a level of 71.8 m asl down to a minimum

Fig. 2. Complete time series of monthly-averaged daily measurements of Mar Chiquita Lake water level, from November 1967 to September 2017. Data analyzed in the present work cover the period 2003–2017.

of 67.1 m asl in October 2013, followed by a recent progressive recovery reaching a level of 69.8 m asl in September 2017. As it was referred to, water levels higher than about 66 m asl imply flooded area in the surroundings of Mar Chiquita Lake, and they constitute the main subject of analysis in this work.

3.2. Satellite pixel classification

The whole Dulce River wetlands region analyzed in this work is topographically flat and it basically lacks of artificial features, so it is free of mountains' shadows and urban areas that often cause misclassification of water mapping due to similar reflectance patterns (Feyisa et al., 2014; Verpoorter et al., 2012). Two sub-areas, whose contours remain basically stable during long periods of time, were selected to define the MNDWI thresholds for pixel classification: Los Porongos lagoon (Fig. 1-right and observed in detail in Fig. 3-top) and MC South Cove (Fig. 1-right and observed in detail in Fig. 3-bottom). The detection of mixed-water pixels composed by soil and/or vegetation with a given percentage of water is a more complex subject when data from only one sensor are used. A deeper analysis of moist soil and mixed pixels would request complementary data such as synthetic aperture radar (SAR) measurements (e.g. Xiao et al., 2014; Mitchell et al., 2015) which are not in the scope of this work. Other studies for biodiversity monitoring include the complement with atlas of habitat-specific plant species (e.g. Kosicki and Chylarecki, 2013), essential biodiversity variables (Vihervaara et al., 2017), etc. Evidently, MNDWI for mixed pixels will take intermediate values between the positive and the negative mode of the distribution, and a variety of approaches have been implemented in previous studies to define these thresholds (e.g. Acharya et al., 2016; Jones, 2015; Ho et al., 2011, 2010; Ji et al., 2009). As this work deals with flooded areas, the identification of mixed pixels is crucial. For this purpose, MNDWI values were analyzed for all dates listed in Table 2 along straight-line transects crossing Los Porongos lagoon and MC South Cove (highlighted over the MNDWI images in Fig. 3-right).

The MNDWI pixel values along the transects for the sixteen available dates (listed in Table 2) of L8-OLI and L5-TM scenes are plotted in Fig. 4, assuring a contrast between water and non-water pixels which are separated by a steep transition from land to open water in the rather stable water body's borders, leaving an intermediate range of MNDWI values that can be considered as mixed pixels. In Fig. 4, some peaks on the terrain at both sides of Los Porongos lagoon are consistent with the presence of temporary streams or non-permanent small pools between scrubland appearing during rainy periods. These pixels had no incidence since they were excluded from the analysis, as explained bellow.

The MNDWI thresholds to separate mixed-water pixels from open-water pixels and non-water pixels were obtained through a box-plot analysis, observed in Fig. 5-left for Landsat 5 TM, Fig. 5-right for Landsat 8-OLI. It results from the "horizontal" sections with small variability of MNDWI values from Fig. 4, associating lower values to non-water pixels and higher values to open-water pixels, excluding those pixels along the jump of transition and those mentioned peaks on the terrain belonging to non-permanent pools and streams. From Fig. 5, the MNDWI box plots corresponding to open-water pixels and non-water pixels are well separated for both sensors, and T-Student test was performed to compare their mean values which resulted significantly different with 95% of confidence ($p < 0.05$) in both cases. In Fig. 5, horizontal dashed lines indicate the thresholds that represent the mixed-water pixels range for both sensors. They are detailed in Table 3.

In addition, Fig. 6 distinguishes the ranges detailed in Table 3 on the histograms of MNDWI pixel values from the whole Los Porongos region for the February 2010 L5-TM image and for the April 2013 L8-OLI image. Fig. 7 shows the classified images of Los Porongos region for both the L5-TM 2010 (Fig. 7-top) and the L8-OLI 2013 (Fig. 7-bottom), standing out the water bodies in black colour. Fig. 7-left shows the
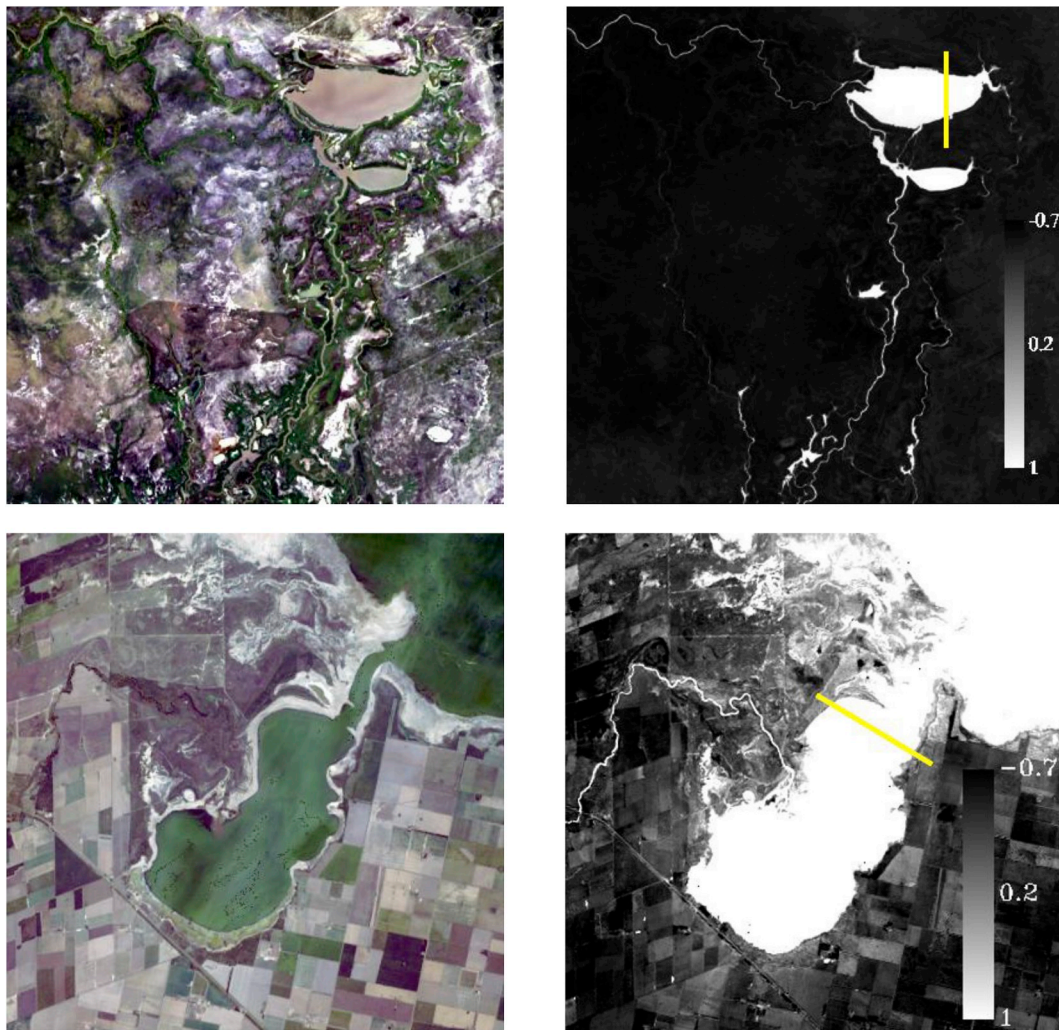
Fig. 3. Sub-area of the L8-OLI 2013 image corresponding to Los Porongos lagoon (**Top**, upper rectangular contour in Fig. 1-right) and MC South Cove (**Bottom**, lower rectangular contour in Fig. 1-right) used to determine the criteria for water pixel classification. **Left:** real colour (RGB-432). **Right:** MNDWI image where water areas stand out in light tones. Geographical transects used to determine the MNDWI thresholds are demarked as yellow segments over both water bodies.

mixed-water classified images, Fig. 7-center shows the open-water classified images and Fig. 7-right shows the total (open + mixed) water classified images. Once the number of water-representing pixels are counted, the total area covered by water within the study zone is obtained multiplying by the 900 m^2 area of each pixel.

3.3. Validation

3.3.1. Use of higher-resolution images

Fig. 8 shows cut-out images of Los Porongos lagoon from three sources with different spatial resolution: Landsat 8-OLI scene from April 16, 2013 (Fig. 8-left), SPOT5-HGR scene from 08 April 2013 with a spatial resolution of 10 m (Fig. 8-center) and a cut-out from Google Earth platform corresponding to a CNES/Airbus image from 2018, with a spatial resolution of 0.5 m (Fig. 8-right). Check points were extracted from the SPOT image, close in date to assure that changes in water conditions on the ground between satellite acquisitions were minimized to validate the open-water, non-water and mixed-water Landsat 8-OLI classification. This is a very important issue since the water content over the flooding area in this region is highly variable and images too sparse in time do not allow feasible comparisons. So, given that we do not have access to dates close to Landsat 8-OLI passes for the highest spatial resolution CNES/Airbus image, it can't be used to extract check points. It was only used as a complement to observe details over the

validation zone and to analyze MNDWI peaks at the boundaries of the lagoon along the transect used to determine the thresholds (Fig. 3-top).

Fig. 8-center shows the sampling check points selected from the SPOT image to be used as ground truth, where open-water pixels are coloured in blue, non-water pixels in green, and mixed pixels in red. Mixed-water pixels were selected point by point following the lagoon and river margins from the RGB (121) composite, while open-water and non-water areas were extracted as polygons. It is worth noting that, due to their different spatial resolution, nine pixels in a SPOT image cover the area of one pixel in a Landsat 8-OLI image. A total of 7938, 1701 and 4194 pixels were collected from the SPOT image as non-water, mixed pixels and open-water samples respectively, corresponding to 882, 189 and 466 control points in the Landsat 8-OLI scene (Fig. 8-left). Table 4 presents the confusion matrix results, showing excellent agreement with an overall accuracy of 99.2% (Equation (2)) and a Kappa coefficient of 0.98 (Equation (3)). Table 5 shows the commission and omission errors for each class. Non-water, mixed-water and open-water pixels present very small commission errors of 0.6%, 0% and 1.3% and omission errors of 0%, 6.4% and 0% respectively.

Now, we simulate the MNDWI values as result of their non-water and open-water fractions in order to evaluate the minimum and maximum content of water present in a Landsat 8-OLI pixel to be classified as mixed-water. This approach has been used for MNDWI calculated for several sensors using the assumption of the linear mixture model, which
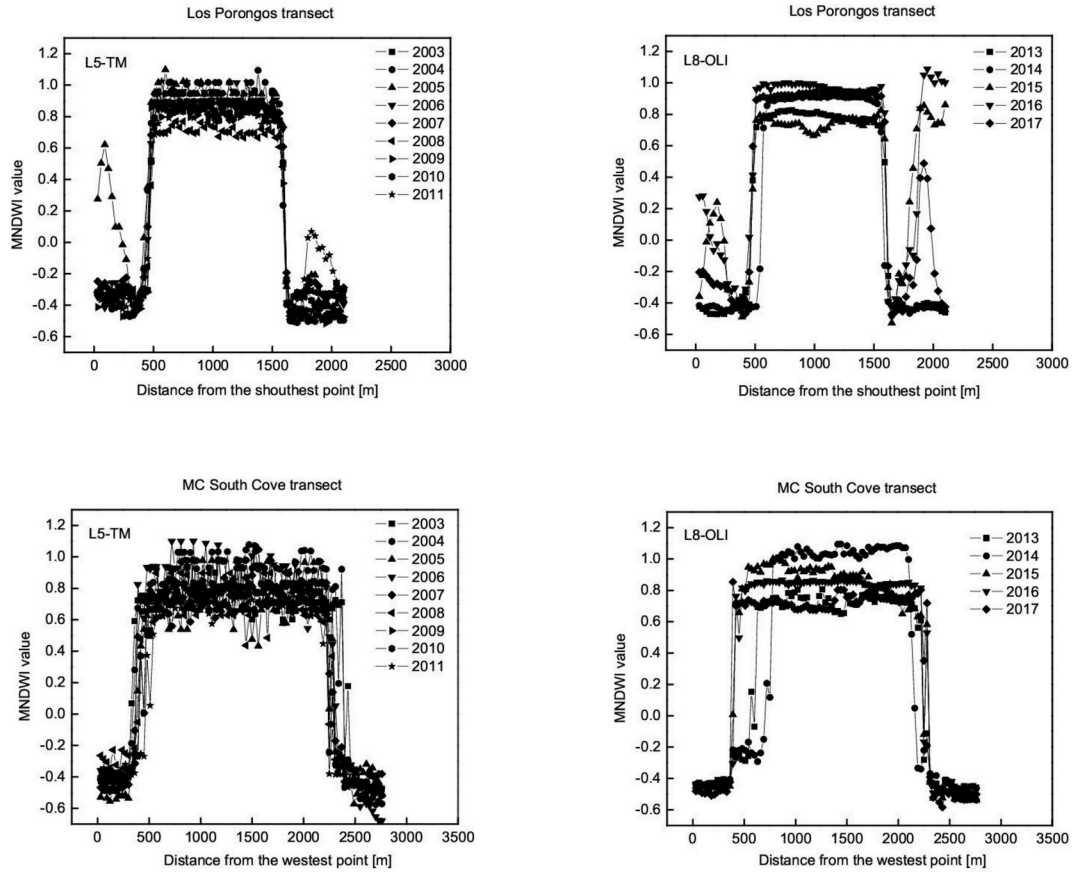
Fig. 4. MNDWI values as a function of distance from a starting point along both transects of Fig. 3, for the scenes covering the whole range of dates of Table 2. **Top:** Los Porongos transect (South-North direction). **Bottom:** MC South Cove transect (West-East direction). **Left:** Landsat 5-TM data. **Right:** Landsat 8-OLI data.

states that the different components in a pixel contribute independently to its reflectance (Ji et al., 2009), giving in our case the equation:

$$\text{Simulated MNDWI} = -0.45 * f_{non-water} + 0.8 * f_{open-water} \quad (4)$$

where $f_{non-water}$ and $f_{open-water}$ correspond to the fraction of non-water area and open-water area respectively inside a pixel classified as mixed-water. Coefficients -0.45 and 0.80 are in fact the obtained Landsat 8-OLI mean values of the MNDWI distributions for these pure-content features (square symbols in the box-plots of Fig. 5-right). Fig. 9 presents simulated MNDWI Landsat 8-OLI values calculated from Equation (4), inferring that mixed-water pixels calculated using the thresholds of Table 3 should contain from about 9% to 76% of their area covered by open-water.

To check the simulated MNDWI, the inner open-water content was analyzed in Landsat 8-OLI pixels classified as mixed-water at the boundaries of Los Porongos lagoon by comparing with the classification (using the same thresholds than L8-OLI from Table 3) of the nine SPOT

pixels contained in each Landsat 8-OLI pixel. Fig. 10 a) shows a MNDWI image calculated for the SPOT5-HRG2 cut-out by using band 1 (centered at 545 nm) and band 4 (centered at 1665 nm). Fig. 10 b) presents MNDWI values along Los Porongos transect for both sensors, L8-OLI and SPOT5-HRG2. It can be observed that jumps across the boundaries of Los Porongos lagoon appear at the same distance and mixed pixels for HRG2 sensor present a range between 0 and 0.55. Recently, Ogilvie et al. (2018) presented a semi-automated method to assess and optimize the potential of multi-sensor Landsat time series to monitor surface water extent and mean water availability over small water bodies in Tunisia. They used SPOT imagery and hydrometric field data of the period 1999–2014 for seven small reservoirs to calibrate MNDWI thresholds which resulted, out of other six water detection indices, to provide high overall accuracy and threshold stability during high and low floods. They obtained a mean surface area error below 15%, attributed mainly to undetected narrow inlets on certain lakes. They propose an optimal threshold to delineate water bodies equal to -0.09,
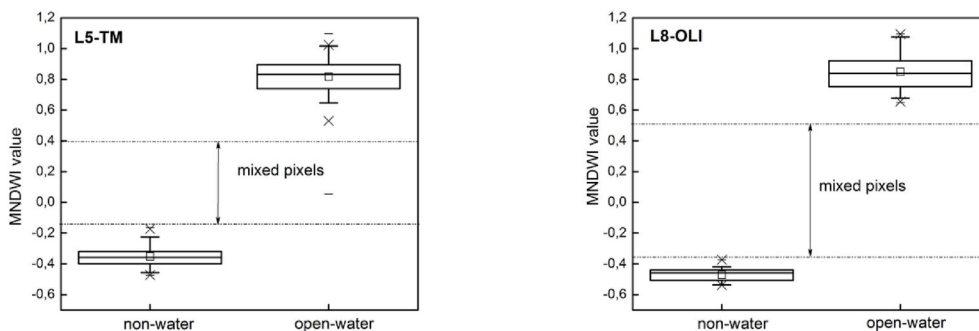
Fig. 5. Box-plot analysis of MNDWI values for definite conditions of open-water and non-water from all dates and both transects of Fig. 4 that allow determining the thresholds for the classification of mixed-water pixels, demarcated as horizontal dash lines and also detailed in Table 3. **Left:** from Landsat 5-TM data. **Right:** from Landsat 8-OLI data.
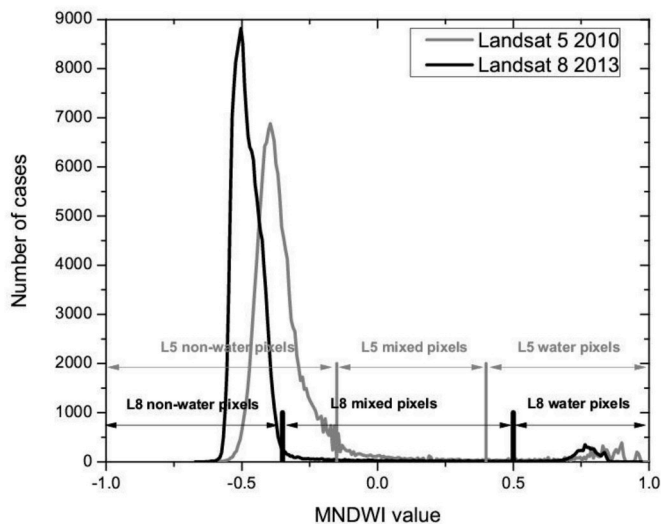
Fig. 6. Histograms of MNDWI pixel values for the Landsat 5-TM 2010 and Landsat 8-OLI 2013 images from data of the whole Los Porongos lagoon region (upper rectangular contour in Fig. 1-right). Vertical lines denote the MNDWI thresholds established in Table 3 for the three cases: non-water pixels, mixed-water pixels and open-water pixels.

and based on their previous experience they suggest that this value includes mixed pixels. In our study we used a threshold of 0.5 to calculate open-water pixels from the SPOT MNDWI image. This threshold is slightly larger than the recommended by Ji et al. (2009): values greater than cero to detect water from SPOT 5 MNDWI data. Fig. 10 c) shows the SPOT 5 MNDWI image, with the SPOT mixed-water pixels highlighted in red colour and a black square contour corresponding to a

Landsat pixel classified as mixed-water containing nine SPOT pixels. Fig. 10 d) presents in cyan colour the SPOT MNDWI pixels classified as open-water within the region delineated as mixed pixels in a Landsat 8-OLI coarser classification. This classification was also revised by visual analysis over a SPOT composite (322), in which the lagoon boundaries are clearly defined. The black square contour in Fig. 10 d), corresponding to the mixed-water-classified Landsat pixel centered at 30° 02′ 57.86″ S, 62° 38′ 19.48″ W, shows that the presence of 100 m^2 of open water (a SPOT-pixel area), which corresponds to 11% of a Landsat pixel area, is enough to detect a Landsat mixed-water pixel using the thresholds from Table 3. This result is consistent with the MNDWI simulation (Fig. 9) suggesting a minimum of about 9% of open-water content to classify mixed pixels according to Table 3. To round off, a L8-OLI pixel centered at 30° 02′ 55.26″ S, 62° 38′ 16.13″ W containing six open-water-classified SPOT pixels (66% of its area, just below the limit of 76% deducted from Fig. 9) is also classified as mixed-water.

3.3.2. Context with similar works

In a recent study, Acharya et al. (2018) compared five methods, based on water spectral indices, to infer flooded areas in Nepal, finding that MNDWI is reliable to detect mixed pixels of small ponds and rivers but unable to detect snow cover and shadows in the Himalayas, errors that are absent in our study zone, free of shadows and snow. They did not discriminate between mixed pixels and open-water to classify water bodies and they proposed an optimal threshold equal 0.35, which is consistent with our results but would overestimate the open-water area in our region. Feyisa et al. (2014) performed a thorough study of water indices evaluation with Landsat 5-TM imagery and proposed a new one. They have also demonstrated that a MNDWI threshold equal to 0.5 to classify open-water pixels presents an accuracy of 81%, containing inside at least 50% of detectable open water. In our study zone, pixels with 50% of water content are classified as mixed within a 94% of
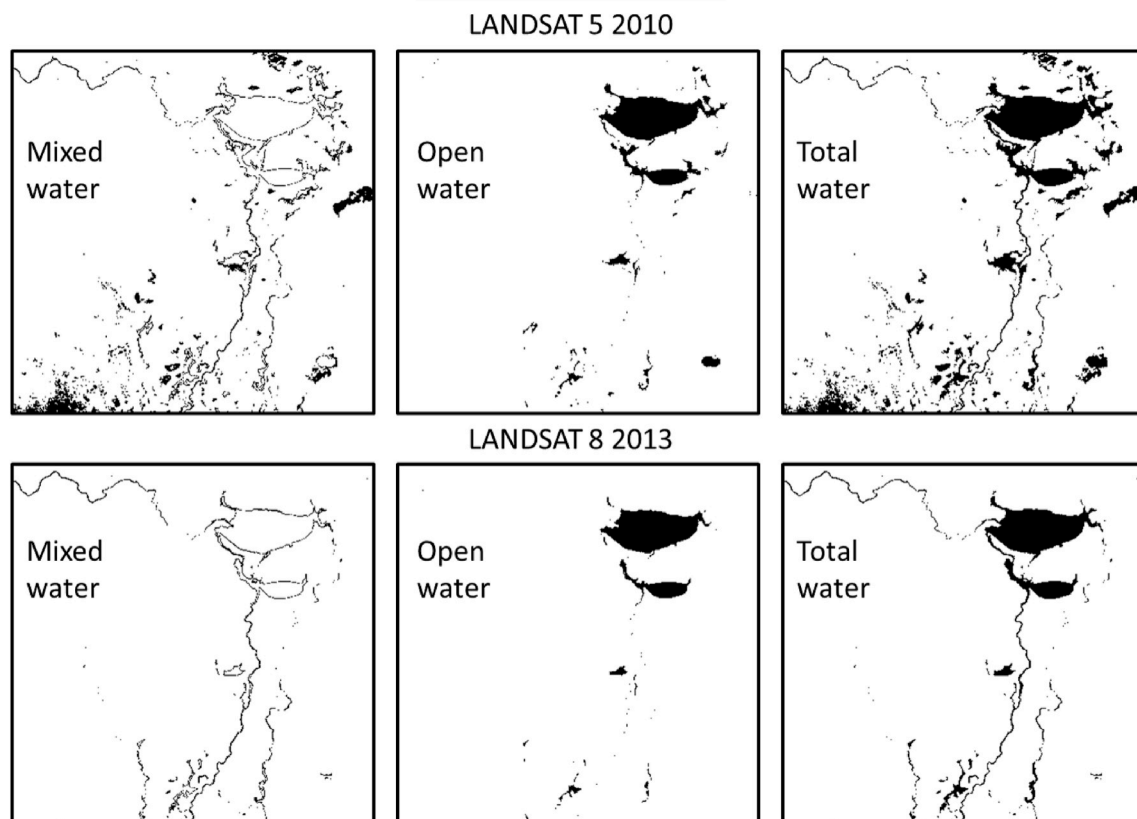
Fig. 7. Classified images of Los Porongos lagoon region according to the MNDWI ranges defined in Table 3. **Top:** Landsat 5, 12 February 2010. **Bottom:** Landsat 8, 25 April 2013. **Left:** mixed-water pixels. **Center:** open-water pixels. **Right:** total (mixed + open) water pixels.
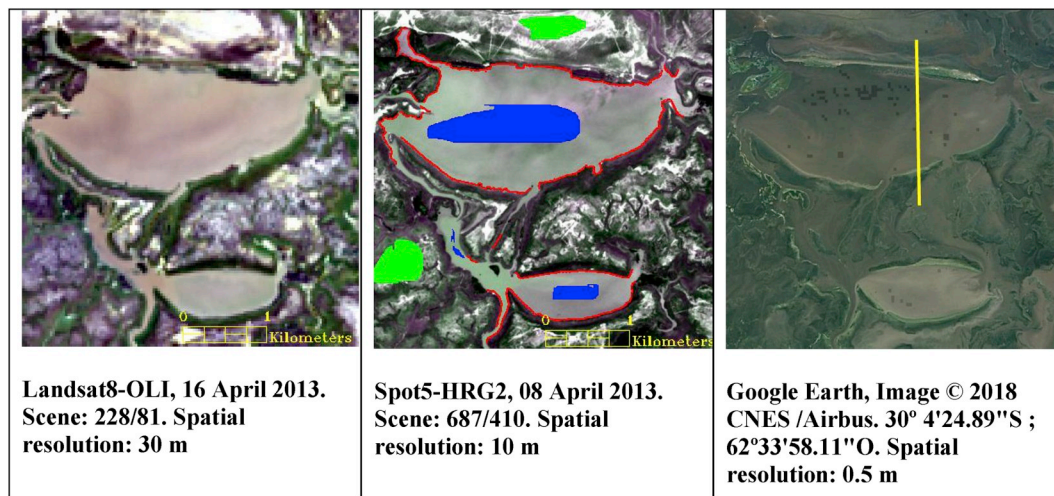
Fig. 8. Cut-out images of Los Porongos lagoon from three sources with different spatial resolution. **Left:** Landsat-8 OLI (RGB, 432) 16 April 2013 used as the test zone for validation. **Center:** SPOT 5-HGR2 (RGB, 121) 08 April 2013 used to select ground truth points: non-water pixels (green), open-water pixels (blue) and mixed-water pixels (red). **Right:** High spatial resolution Image © 2018 CNES/Airbus, taken from Google Earth facilities. Vertical yellow line corresponds to Los Porongos transect.

Table 4
Confusion matrix obtained from the SPOT image dated on 08 April 2013 at check sites shown in Fig. 8-center and thresholds classification according to Table 3. Overall Accuracy = 99.2%, Kappa coefficient = 0.98.
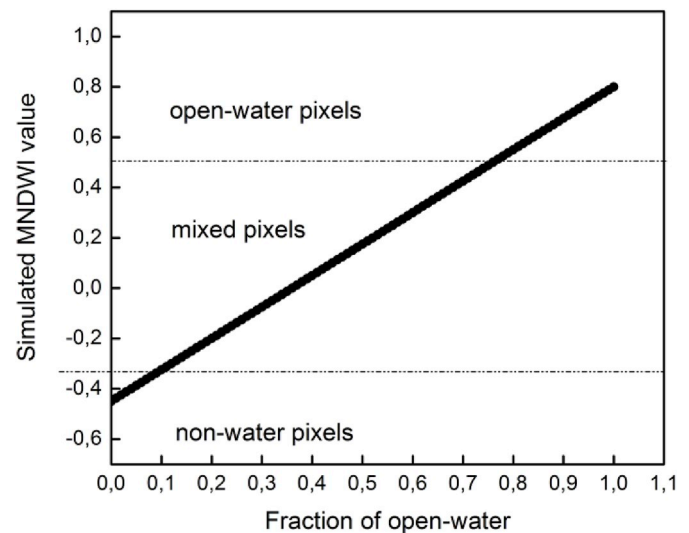
Class	Ground truth pixels taken from SPOT image			
	Non water	*Open water*	*Mixed pixels*	*Total*
Unclassified	0	1	0	1
Non water	882	5	0	887
Mixed pixels	0	177	0	177
Open water	0	6	466	472
Total	882	189	466	1537

Table 5
Commission and omission errors for each class of classification, resulting from the analysis of Table 4.

Class	*Commission error (%)*	*Omission error (%)*
Non water	0.6	0
Mixed pixels	0	6.4
Open Water	1.3	0

Fig. 9. Simulated Landsat 8-OLI MNDWI values from the linear mixture model (Equation (4)) which allows estimating the range of detectable open-water fraction of area inside a given pixel to be classified as mixed-water. They are demarked as dashed horizontal lines at open-water fractions of 0.09 and 0.76.

confidence using the same threshold. Martins et al. (2018) evaluated the surface water change and turbidity variability of Sobradinho reservoir in northern Brazil during drought years, from 2013 to 2017, by analysing Landsat 8-OLI time series. They classified pixels as open-water if the MNDWI > 0 and NDVI < 0 and they did not include mixed pixels in their analysis. However, the threshold value equal to zero was determined on a preliminary assessment over five land-cover categories, i.e. clear water, turbid water, vegetation, soil/sand and urban surfaces. In addition, they present box-plot analysis of MNDWI index values for clear and turbid open-water covers which are concentrated over 0.5, in agreement with the results of the present work. The review by Boschetti et al. (2014) compares the performance of several water indices for MODIS sensor, finding that MNDWI, calculated from band 4 (Green) and band 6 (SWIR) showed the best performance, proposing a threshold for open water equal to −0.228. In that case, according to a second order adjustment between MNDWI and water content with a determination coefficient equal to 0.59, that value would indicate near 40% of water content inside a pixel. They have demonstrated that MNDWI index presents the third best performance among VIR/SWIR

and VIS/NIR indices to detect open-water pixels. Finally, Fisher et al. (2016) evaluated six different water indices, including MNDWI, to perform automatic water body extraction in eastern Australia. They demonstrated, based on long term data, that all indices and thresholds perform consistently across images from different Landsat sensors (TM, ETM+ and OLI) facilitating the automated classification of water bodies to similar levels of accuracy for the growing archive of Landsat data, consistently with the results of the present work. Finally, Crétaux et al. (2016) proposed methodological approaches to monitor lake-volume from space, particularly by SAR altimetry measurements, using also MNDWI index applied to Landsat 5-TM and MODIS sensors to infer lake areas. They established that final conclusions will depend on the methodology employed and the study zone delineation, emphasizing the need of validation with ground observations if available. In this framework, we had also performed a field campaign simultaneously with a Landsat 8-OLI overpass to assess the precision of the classification.
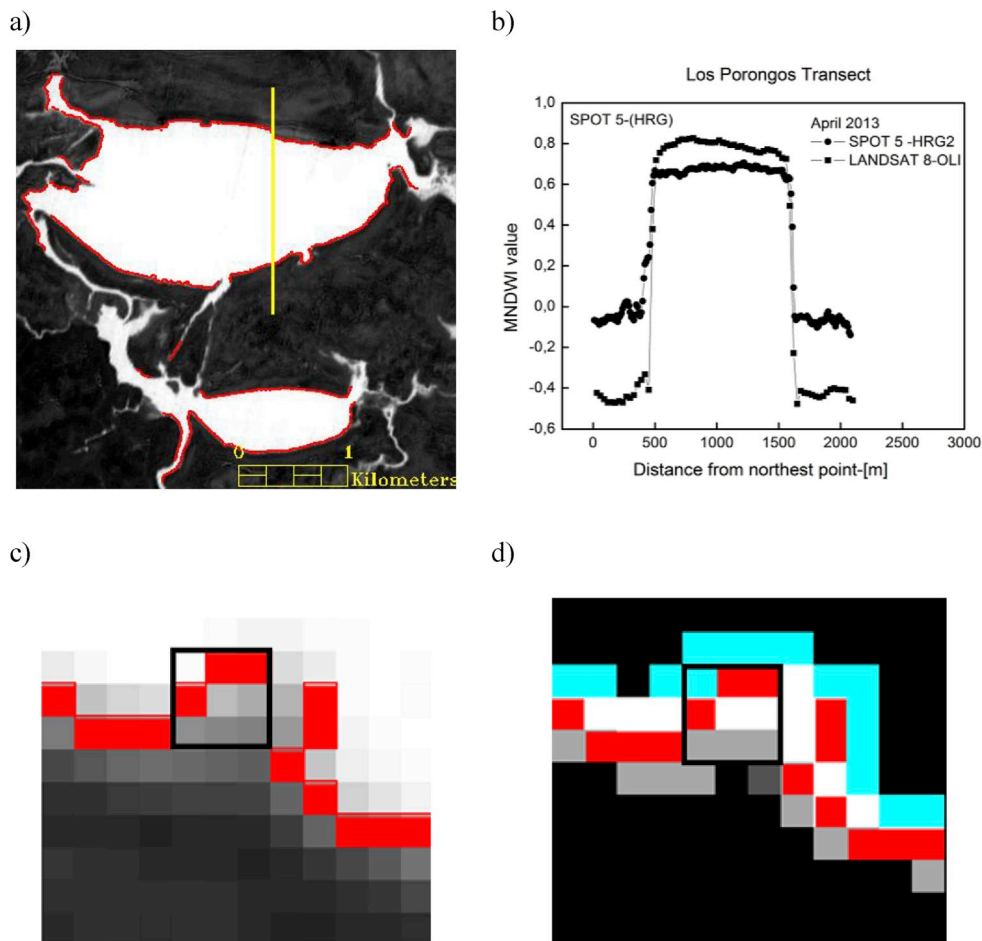
Fig. 10. a) SPOT 5-HRG2 MNDWI image calculated for Los Porongos lagoon region. Red points correspond to mixed-water pixels selected as ground truth for the validation process. **b)** SPOT-5 and Landsat 8 MNDWI values as a function of distance along Los Porongos transect (yellow line). **c)** SPOT 5 MNDWI image with mixed-water pixels in red colour and a selected Landsat 8 mixed-water pixel (black square contour, centered at 30° 02′ 57.86″ S, 62° 38′ 19.48″ W). **d)** The same Landsat 8 mixed-water-classified pixel, shows that it contains only one SPOT open-water-classified pixel (highlighted in cyan colour), in the lower limit deducted from Fig. 9.

3.3.3. Photographic field assessment

In-situ GPS-georeferenced digital photographic registers were taken at many sites in a field itinerary along a Northwest zone of the Nature Reserve (see Fig. 1-right) during morning hours of day 06 April 2015, simultaneous to a Landsat 8 overpass, for different ground conditions including dry and wet soil, pure vegetation, mixed areas with different proportions of water, and open-water lagoons, which are used as a complement to validate the satellite image classification. The sky was partially cloudy with sparse cumulus (total cloud cover of the whole Landsat scene: 8%). Then, digital pictures taken at sites where the Landsat 8 scene presented neither cloud nor cloud shadow were selected for the comparison.

Fig. 11 presents examples of the photographic validation showing very good agreement with the MNDWI thresholds defined for satellite pixel classification, under the three ground conditions we need to distinguish within a wetland region: open water pixels, mixed pixels with different proportions of observed water, and non-water pixels. It can be observed that the defined mixed water pixels range within $-0.35 <$ MNDWI < 0.5 for L8-OLI is in fact appropriate, given that pixels mostly covered by mud, vegetation and soil have MNDWI values just below the threshold of -0.35. Even though no similar photographic registers are available in previous years, the L5-TM MNDWI thresholds were established with the same criteria as seen in Figs. 4 and 5, and the limit MNDWI $= 0.4$ to separate mixed-water from open-water pixels for L5-TM was selected as the minimum MNDWI value assuring that the interior of Los Porongos lagoon being classified as

open-water. Note that the third photo from left column is classified as non-water, even when it presents some observed water that, as shown, does not cover the minimum of 9% of observed open water necessary to classify a pixel as mixed-water (81 m^2 over the 900 m^2 of a Landsat pixel), supported by the high resolution image analysis which revealed an omission error of only 6.4% in detection of mixed-water pixels (Table 5). Additionally, the MNDWI value for this pixel (-0.379) is very close to the MNDWI value for the fourth photo from left column (-0.370) which corresponds definitely to non-water (prevailing mud with sparse vegetation), ratifying the reliability of the range $-0.35 <$ MNDWI to separate non-water from mixed-water pixels.

3.4. Flooded-area variability analysis

As mentioned above, a total of sixteen Landsat mosaics (Table 2) covering the *Dulce River wetlands and Mar Chiquita Lake* Nature Reserve region in Argentina were analyzed spanning the period 2003–2017. Fig. 12 shows examples of them. Fig. 12-top is in real colour (RGB-321 for L5-TM, years 2003 and 2010, and RGB-432 for L8-OLI, years 2013 and 2015). Fig. 12-bottom highlights in black colour the presence of open water, and in light gray the mixed-water pixels within the Dulce River wetlands under study (see Fig. 1-right), with the Nature Reserve contour and Mar Chiquita Lake area demarcated in dark gray tone.

Fig. 13-left shows the time evolution of the satellite-retrieved extension of open-water, mixed-water and total (open + mixed) flooded area during the analyzed period 2003–2017, together with the locally-

Coordinates: 30°11'3.8''S, 63°9'13.9''W	Coordinates: 30°11'1.6''S, 63°0'6.1''W
Observed ground conditions: shrubs	Observed ground conditions: pool between scrubland
MNDWI value: -0.468 (Satellite classification: non-water)	MNDWI value: -0.331 (Satellite classification: mixed-water)

Coordinates: 30°11'2.8''S, 63°0'7.2''W	Coordinates: 30°11'22.4''S, 63°15'55.4''W
Observed ground conditions: scrubland	Observed ground conditions: prevailing water surrounded by mud
MNDWI value: -0.419 (Satellite classification: non-water)	MNDWI value: -0.329 (Satellite classification: mixed-water)

Coordinates: 30°11'8.6''S, 63°17'38.5''W	Coordinates: 30°10'59.8''S, 65°56'52.8''W
Observed ground conditions: prevailing vegetation with sparse water	Observed ground conditions: prevailing water surrounded by mud
MNDWI value: -0.379 (Satellite classification: non-water)	MNDWI value: -0.27 (Satellite classification: mixed-water)

| Coordinates: 30°11'8.6''S, 63°18'10.6''W	Coordinates: 30°11'34.6''S, 63°14'59.1''W
Observed ground conditions: prevailing mud with sparse vegetation	Observed ground conditions: prevailing water surrounded by mud
MNDWI value: -0.370 (Satellite classification: non-water)	MNDWI value: -0.205 (Satellite classification: mixed-water)

Fig. 11. Examples of field validation of the Landsat 8 MNDWI values obtained from a L8 scene with date 06 April 2015, particularly for non-water and mixed-water pixels, compared with eight geo-referenced digital photographic registers simultaneous to the L8 overpass taken during a field campaign along a Northwest zone (demarcated in Fig. 1-right) within the Nature Reserve. Results ratify the MNDWI ranges defined in Table 3.
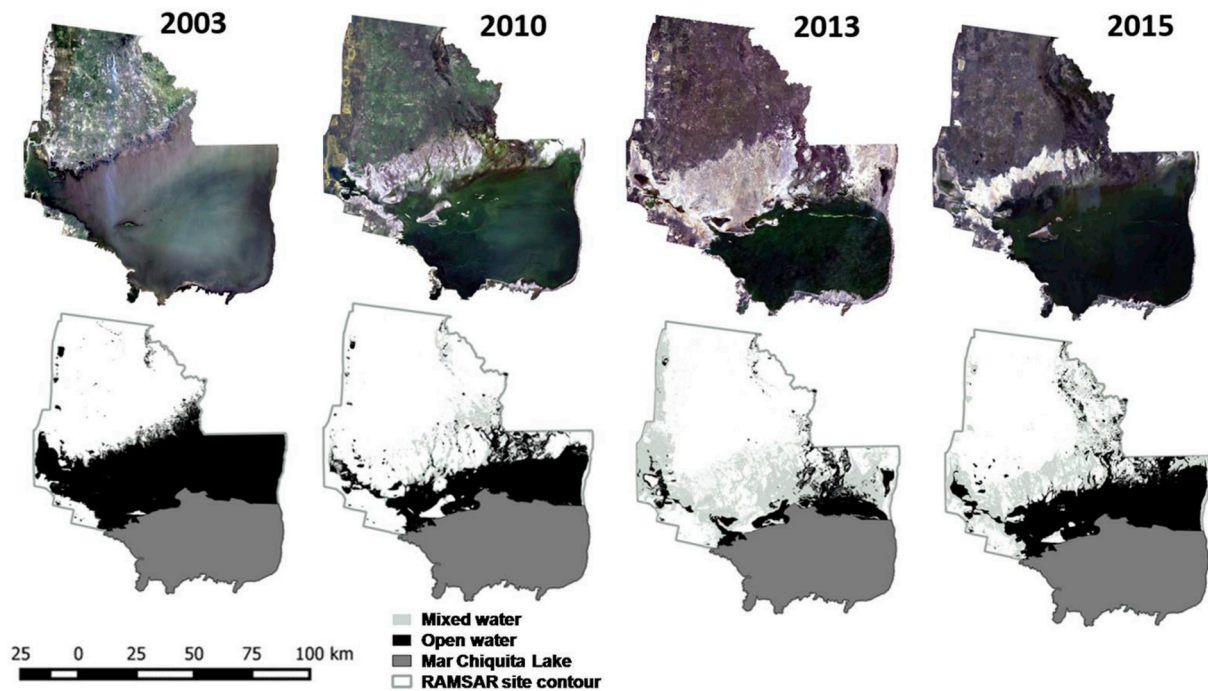
Fig. 12. The *Dulce River wetlands and Mar Chiquita Lake* Nature Reserve in Argentina contoured from mosaics of available cloudless-sky Landsat satellite images dated in December 2003, February 2010, April 2013 and September 2015. **Top:** real colour (RGB-321 for L5-TM, years 2003 and 2010, and RGB-432 for L8-OLI, years 2013 and 2015). **Bottom:** open-water bodies within the Dulce River wetlands are highlighted in black colour and mixed-water pixels in light gray colour, while dark gray tone denotes the Nature Reserve contour and defined filled area of Mar Chiquita Lake at a level of 66 m asl.

measured average water level of Mar Chiquita Lake for the same dates. Open-water and water level follow a strongly correlated behavior, as it is analyzed in detail in Fig. 13-right. Total-water shows its maximum covered area around 2003–2005 with about 3600 km². Open-water area reduced 86% from 3448.54 km² in 2003 (the year of maximum recorded open-water extension with an average water level of 71.8 m asl in May 2003) down to 478.57 km² by the end of 2013 (when average water level reached a minimum around 67.5 m asl). As it is expected for a flat basin, the reduction in the area initially covered by open water pixels due to different processes (e.g. hydrological deficit, evaporation in absence of rain, absorption by the soil) implies that many of them change to an intermediate condition of mixed-water, increasing the fraction covered by mixed water pixels within the same area simultaneously, and the reduction in the area covered by open water implies an increase in the area covered by mixed water as shown in Fig. 13-left. However, this increase in the area covered by mixed water has two well defined periods. Even though the open-water covered area diminishes constantly in the period 2003–2013, mixed water shows a slowly rather linear increase

from 2003 to 2011 followed by a sudden increase from 2011 to 2013 when it reaches their maximum. In turn, 2011 agrees with the date when the total water (open + mixed) reaches their minimum (2056.1 km²) and their recovery starts at a rather constant rate until 2015–2017 with an extension of about 3400 km², when the Mar Chiquita Lake water level (see Fig. 2) reaches 69.80 m asl in September 2017. Then, period 2011–2013 is key to understand the phenomena: after a period (2003–2011) of negative hydrological balance by reduced contribution from the northern rivers, a positive hydrological balance started in 2011 when the northern rivers increased their caudal. The first result of this positive hydrological balance is the increase in the mixed-water areas from the north when water is starting to recover the region, even though open-water area still reduces during the period 2011–2013. After 2013, this increased caudal incorporates to the open-water area at the north of Mar Chiquita Lake which starts their recovery in detriment of the mixed-water that loses the area gained by the open-water, while the total-water area continues their increase until 2015–2017 with an area of about 3400 km².
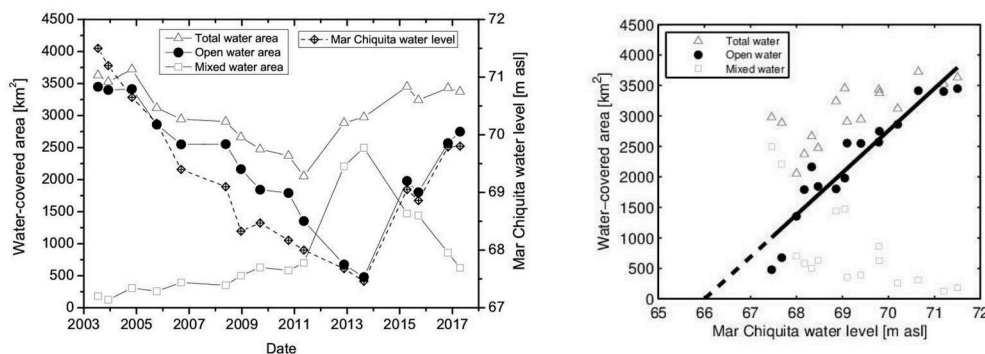
Fig. 13. Left: Time evolution of the satellite-retrieved flooded-area extension within the Dulce River wetlands for the cases of mixed water, open water and total (mixed + open) water, and simultaneous locally-measured average water level of Mar Chiquita Lake during the period 2003–2017. **Right:** Satellite-retrieved flooded area within the Dulce River for open-water, mixed water and total water as a function of the average water level of Mar Chiquita Lake. Solid black line represents a linear fit to the open-water data, giving a slope s = 690 ± 72 km²/m, while dashed black line is a linear extrapolation of the fitting down to zero flooded area, which would be reached for a water level of 66.0 m asl.

Fig. 13-right shows that the area covered by open-water pixels is strongly linearly correlated (correlation coefficient $r = 0.95$, p-value $= 6\,e-8$) with the Mar Chiquita Lake water level, different from the mixed water pixels ($r = -0.70$, p-value $= 4\,e-3$) and the total flooded area ($r = 0.77$, p-value $= 7\,e-4$). The resulting linear fit of open-water pixels as a function of Mar Chiquita Lake water level (coefficient of determination $r^2 = 0.90$) is consistent with two independent observations. Firstly, the linear extrapolation to zero-flooded-area within the Dulce River wetlands is obtained for a Mar Chiquita water level of 66.0 m asl, effectively the mentioned level of about 66 m asl that defines the Mar Chiquita Lake contour. Secondly, a slope $s = 690 \pm 72\,km^2/m$ (at one standard deviation confidence level) is obtained in the linear fit. If the maximum flooded area in the Dulce River wetlands during year 2003 is approximated by a rectangular surface (in nadir view) with longest side $L \approx 80\,km$, oriented slightly Southwest-Northeast as shown in Fig. 14, it can be deduced that the topographical percentage slope α of the Dulce River mouth wetlands, idealized as a plain tilted terrain, is $\alpha = 100*L/s$. So, $\alpha \approx 0.012\%$ is obtained in agreement with the value of $\alpha < 0.02\%$ determined from bathymetric studies of the same area (Vargas, 2014).

Fig. 14. Simplified rectangular area of longest side $L = 80$ km (in nadir view) representing the maximum extension of the open-water Dulce River wetlands flooded area over an idealized plain tilted surface of percentage topographical slope α, plotted over the satellite-retrieved open-water flooded area (highlighted in black colour) during the maximum extension of year 2003 within the Nature Reserve. Considering the slope $s = 690 \pm 72\,km^2/m$ of the linear fit from Fig. 13-right, the resulting value is $\alpha \approx 0.012\%$.

4. Conclusions

This work constituted a practical application of satellite data complemented by a set of locally-measured parameters and registers for analysis and validation, integrating scientific and official decision-maker institutions for monitoring, understanding and preservation of a wetland Nature Reserve of international relevance in Argentina. The water-covered surface area within the potentially flooded region of the Ramsar Nature Reserve *Dulce River wetlands and Mar Chiquita Lake* in Córdoba Province, Argentina, was retrieved from L5-TM and L8-OLI reflectance data by using the Modified Normalized Difference Water Index (MNDWI) on a total of 16 cloudless-sky mosaics in the period 2003–2017. As in every wetland region, the sensitivity of the satellite algorithm to detect areas partially covered by exposed water or with underlying water is crucial, and especial emphasis to correctly classify mixed-water pixels has been put in this work. Transects crossing two stable sub-regions, Los Porongos lagoon and a South branch of Mar Chiquita Lake, were used with the sixteen available image dates to define through box-plot analysis the MNDWI threshold values for each sensor to detect open-water pixels, mixed-water pixels and non-water pixels. To validate the established satellite MNDWI thresholds, a SPOT higher resolution satellite image was used, complemented by digital photographic registers taken within the Nature Reserve simultaneously to a Landsat 8 overpass, covering a diversity of zones with different proportion of observed water, assuring reliability in distinguishing mixed-water pixels. Additionally, an exhaustive linear mixture model analysis of the percentage of detectable open water inside a given Landsat pixel was made, ranging from 9% to 76% to be classified as a mixed-water pixel.

Maximum total flooded area extensions of about $3600\,km^2$ during years 2003–2005 and a minimum one of $2050\,km^2$ by the end of 2011 were determined. Supporting the known phenomenology of the region, the comparative evolution of open-water, mixed-water and total-water areas, and the Mar Chiquita Lake water level is highly compatible with an explanation that strongly relates the hydrological balance in the region with the caudal regime from the contributing northern rivers. The satellite-estimated open-water flooded area within the Dulce River wetlands shows a marked linear relation with the average locally measured water level of Mar Chiquita Lake. The extrapolation of the linear fitting to zero flooded area closely agrees with the water level of about 66 m asl that defines the historical contour of Mar Chiquita Lake. Idealizing the Dulce River wetlands as a rectangular plain tilted surface, the slope of the linear fitting ($690\,km^2/m$) leads to a terrain's topographical slope of 0.012%, in agreement with the topographical slope $< 0.02\%$ obtained from bathymetric studies in the same area.

While the open-water flooded area within the Dulce River wetlands decreases systematically since 2003 down to the end of 2013, the total flooded-area reached its minimum by the end of 2011, when a significant increase of the mixed-water area started. The detailed links of this behavior to the whole variables influencing the hydrological balance, climate parameters, chemical and physical water parameters, etc. in this complex endorheic system will be a subject of future work. The analysis of satellite imagery and correlations found in this work can be part of a management tutorial for government officials attending the preservation of the resources within this important Nature Reserve. The validated satellite method here provided constitutes a contributing tool to discriminate mixed-water from open-water pixels for monitoring different aspects of wetlands in the present climate change scenario.

References

Acharya, T.D., Lee, D.H., Yang, I.T., Lee, J.K., 2016. Identification of water bodies in a Landsat 8 OLI image using a J48 decision tree. Sensors 16 (7), 1075. https://doi.org/10.3390/s16071075.
Acharya, T.D., Subedi, A., Lee, D.H., 2018. Evaluation of water indices for surface water

extraction in a landsat 8 scene of Nepal. Sensors (Basel, Switzerland) 18 (8), 2580. https://doi.org/10.3390/s18082580.

Boschetti, M., Nutini, F., Manfron, G., Brivio, P.A., Nelson, A., 2014. Comparative analysis of normalised difference spectral indexes derived from MODIS for detecting surface water in flooded rice cropping systems. PLoS One 9 (2), e88741.

Bucher, E.H., 1992. Population and conservation status of flamingos in Mar Chiquita, Córdoba, Argentina. Colon. Waterbirds 15, 179–184.

Bucher, E.H. (Ed.), 2006. Bañados del Río Dulce y Laguna Mar Chiquita (Córdoba, Argentina). Academia Nacional de Ciencias, Córdoba, Argentina.

Chen, Y., Huang, C., Ticehurst, C., Merrin, L., Thew, P., 2013. An evaluation of MODIS daily and 8-day composite products for floodplain and wetland inundation mapping. Wetlands 33, 823–835.

Congalton, R.G., Green, K., 1999. Assessing the Accuracy of Remotely Sensed Data: Principles and Practices. Lewis Publishers, pp. 137.

Crétaux, J.-F., Abarca-del-Río, R., Bergé-Nguyen, M., Arsen, A., Drolon, V., Clos, G., Maisongrande, P., 2016. Lake volume monitoring from space. Surv. Geophys. 1–37.

Ferral, A., Aleksinkó, A., Plomer, E., Orueta, A., Cossano, N., Bernasconi, I., Díaz, A., Scavuzzo, M., 2013. Detección de cambios temporales de superficie inundada en la zona de la Laguna de Mar Chiquita mediante imágenes satelitales. In: III Congreso Internacional de Ambiente y Energías Renovables, Villa María, Córdoba, Argentina, pp. 44–53.

Feyisa, G.L., Meilby, H., Fensholt, R., Proud, S.R., 2014. Automated Water Extraction Index: a new technique for surface water mapping using Landsat imagery. Remote Sens. Environ. 140, 23–35.

Fisher, A., Flood, N., Danaher, T., 2016. Comparing Landsat water index methods for automated water classification in eastern Australia. Remote Sens. Environ. 175, 167–182.

HGS, 2016. Harris Geospatial Solutions - Product Documentation Center. http://www.exelisvis.com/docs/BackgroundOtherIndices.html.

Ho, T.K.L., Umitsu, M., Yamaguchi, Y., 2010. Flood hazard mapping by satellite images and SRTM DEM in the Vu Gia - Thu Bon alluvial plain, central Vietnam. International archives of the photogrammetry. Remote Sens. Spat. Inf. Sci. 38, 275–280.

Ho, T.K.L., Yamaguchi, Y., Umitsu, M., 2011. Significance of Combining SRTM DEM and Satellite Images for Generating Automated Micro-landform Map, vols. 101–104 Geomorphometry. http://geomorphometry.org/system/files/LoanHo2011geomorphometry.pdf.

Ji, L., Li, Z., Bruce, W., 2009. Analysis of dynamic thresholds for the normalized difference water index. Photogramm. Eng. Rem. Sens. 75, 1307–1317. https://doi.org/10.14358/PERS.75.11.1307.

Jones, J.W., 2015. Efficient wetland surface water detection and monitoring via Landsat: comparison with in situ data from the everglades depth estimation network. Rem. Sens. 7, 12503–12538. https://doi.org/10.3390/rs70912503.

Kosicki, J.Z., Chylarecki, P., 2013. Predictive mapping of Meadow Pipit density using integrated remote sensing data with Atlas of Vascular Plants dataset. Bird Study 60, 500–508.

Li, L., Vrieling, A., Skidmore, A., Wang, T., Muñoz, A.R., Turak, E., 2015. Evaluation of MODIS spectral indices for monitoring hydrological dynamics of a small, seasonally-flooded wetland in southern Spain. Wetlands 35, 851–864. https://doi.org/10.1007/s13157-015-0676-9.

Martínez, D.E., 1995. Changes in the ionic composition of a saline lake, Mar Chiquita, Province of Córdoba, Argentina. Int. J. Salt Lake Res. 4, 25–44.

Martins, V.S., Kaleita, A., Barbosa, C.C., Fassoni-Andrade, A.C., de Lucia Lobo, F., Novo, E.M., 2018. Remote sensing of large reservoir in the drought years: implications on surface water change and turbidity variability of Sobradinho reservoir (Northeast Brazil). In: Remote Sensing Applications. Society and Environment.

Mitchell, A.L., Milne, A.K., Tapley, I., 2015. Towards an operational SAR monitoring system for monitoring environmental flows in the Macquarie Marshes. Wetl. Ecol. Manag. 23 (1), 61–77.

Mozumder, C., Tripathi, N.K., Tipdecho, T., 2014. Ecosystem evaluation (1989-2012) of Ramsar wetland Deepor Beel using satellite-derived indices. Environ. Monit. Assess. 186 (11), 7909–7927. https://doi.org/10.1007/s10661-014-3976-2.

Nores, M., 2011. Long-term waterbird fluctuations in mar Chiquita Lake, central Argentina. Waterbirds 34, 381–388.

Ogilvie, A., Belaud, G., Massuel, S., Mulligan, M., Le Goulven, P., Calvez, R., 2018. Surface water monitoring in small water bodies: potential and limits of multi-sensor Landsat time series. Hydrol. Earth Syst. Sci. 22 (8).

Piovano, E.L., Ariztegui, D., Moreira, S., 2002. Recent environmental changes in Laguna Mar Chiquita (central Argentina): a sedimentary model for a highly variable saline lake. Sedimentology 49, 1371–1384.

Piovano, E.L., Ariztegui, D., Bernasconi, S.M., McKenzie, J.A., 2004. Stable isotopic record of hydrological changes in subtropical Laguna Mar Chiquita (Argentina) over the last 230 years. Holocene 14, 525–535.

Plencovich, G.E., 2011. Simulación hidrológica de los humedales de Mar Chiquita con apoyo satelital. Msc Dissertation. Universidad Nacional de Córdoba, Argentina.

Reati, G.J., Florín, M., Fernández, G.J., Montes, C., 1996. The Laguna de Mar Chiquita (Córdoba, Argentina): a little known, secularly fluctuating, saline lake. Int. J. Salt Lake Res. 5, 187–219.

Sharma, C.S., Mishra, A., Panda, S.N., 2014. Assessing impact of flood on river dynamics and susceptible regions: geomorphometric analysis. Water Resour. Manag. 28 (9), 2615–2638.

Stutz, S., Prieto, A.R., 2003. Modern pollen and vegetation relationships in Mar Chiquita coastal lagoon area, southeastern Pampa grasslands, Argentina. Rev. Palaeobot. Palynol. 126, 183–195.

Troin, M., Vallet-Coulomb, C., Sylvestre, F., Piovano, E., 2010. Hydrological modelling of a closed lake (Laguna Mar Chiquita, Argentina) in the context of 20th century climatic changes. J. Hydrol. 393 (3), 233–244.

UN, 2017. The Global Indicator Framework, Adopted by the General Assembly on the Statistical Commission Pertaining to the United Nations 2030 Agenda for Sustainable Development. A/RES/71/313.

Vargas, C., 2014. Análisis de la dinámica hídrica espacial de la Laguna Mar Chiquita período 2001-2014 (Bachelor's thesis. Universidad Nacional de Córdoba. Facultad de Ciencias Exactas, Físicas y Naturales.

Verpoorter, C., Kutser, T., Tranvik, L., 2012. Automated mapping of water bodies using Landsat multispectral data. Limnol Oceanogr. Methods 10 (12), 1037–1050.

Vihervaara, P., et al., 2017. How Essential Biodiversity Variables and remote sensing can help national biodiversity monitoring. Glob. Ecol. Conserv. 10, 43–59.

Wang, B., Chen, Y., Lü, C., 2015. Evaluating flood inundation impact on wetland vegetation FPAR of the Macquarie Marshes, Australia. Environ. Earth Sci. 74 (6), 4989–5000.

Xiao, X., Wdowinski, S., Wu, Y., 2014. Improved water classification using an application-oriented processing of Landsat ETM + and ALOS PALSAR. Int. J. Control Autom. 7 (11), 355–370. https://doi.org/10.14257/ijca.2014.7.11.35.

Xu, H., 2006. Modification of normalised difference water index (NDWI) to enhance open water features in remotely sensed imagery. Int. J. Remote Sens. 27, 3025–3033.

Xu-kai, Z., Quiong-quiong, L., Baig, A., Hassan, M., 2012. Automated detection of coastline using Landsat TM based on water index and edge detection methods. Second Int. Workshop Earth Obs. Remote Sens. Appl. 153–156.